Influence of thermo-mechanical treatment on the precipitation strengthening behavior of Inconel 740, a Ni-based superalloy

Jun-Hak Oh, Byung-Gil Yoo, and In-Chul Choi
Division of Materials Science and Engineering, Hanyang University, Seoul 133-791, Korea

Michael L. Santella
Materials Science and Technology Division, Oak Ridge National Laboratory, Oak Ridge, Tennessee 37831

Jae-il Jang[a)]
Division of Materials Science and Engineering, Hanyang University, Seoul 133-791, Korea

(Received 6 November 2010; accepted 28 February 2011)

In this work, we have systematically explored the influence of thermo-mechanical treatment on the precipitation behavior and its strengthening in Inconel 740, a relatively new Ni-based superalloy, using specimens on which different levels of stresses were applied at 700 °C. With increasing applied stress, fraction of gamma prime precipitates increased (without significant size change) and nanoindentation hardness was enhanced. The stress effects were discussed in terms of the free energy barrier for heterogeneous nucleation and the prevailing mechanisms of precipitation strengthening.

I. INTRODUCTION

Inconel 740, a relatively new member of Ni-based superalloy family, has been developed for applications to advanced ultra-supercritical steam boiler tubing in fossil power plants.[1,2] As the target steam condition of the new boiler was 375 bar and 700 °C, this alloy was designed to have excellent performances at 700–750 °C; i.e., good microstructure stability, high resistance to coal ash corrosion and oxidation, and high creep-rupture strength (for 100,000 h rupture life at 100 MPa and for component life longer than 20 years).[1,2] Like many other Ni-based superalloys, this Inconel 740 is primarily strengthened by the precipitation of very fine gamma prime (γ') (having an ordered $L1_2$ structure) in the disordered gamma (γ) matrix.[1,2] Thus, the mechanical properties of the alloy are strongly dependent on the size and fraction of the γ' precipitates.

It is generally accepted that the precipitation strengthening in Ni-based superalloys is mainly controlled by cutting mechanism rather than bowing (or typically referred to as Orowan) mechanism[3,4]: Although a pair of $a/2<1\bar{1}0>\{111\}$ dislocations passes through the γ/γ' structure, the first dislocation enters the spherical γ' precipitates with the formation of an anti-phase boundary (APB) and the following dislocation removes it.[5–8] This type of cutting mechanism can be roughly subdivided into two groups; weakly coupled dislocations (WCD or weak pair coupling) model[9] and strongly coupled dislocations (SCD or strong pair coupling) model.[10] In superalloys, the former is typically applied to the case where the size and volume fraction of γ' are small,[9] whereas the latter is known to be more appropriate for the case where the spacing of the dislocation pairs becomes comparable to the particle diameter.[10]

Although many studies have been performed to observe the variations in microstructures and mechanical properties in the thermally aged or crept superalloy specimens, little efforts have been made on the influence of thermo-mechanical treatment at high stress and high temperature. Especially, to our best knowledge, no research on the issue has been conducted for Inconel 740. With this in mind, how the mechanical properties of the Inconel 740 can be affected by the thermo-mechanical treatment was investigated in this study. The results provided important clues for the precipitation behavior and the way in which it may contribute to the strengthening of the material.

II. EXPERIMENTAL DETAIL

The material examined in this study is a commercial grade Inconel 740 (produced at Special Metals Corporation) whose nominal chemical composition (wt%) is 0.03C–25Cr–0.5Mo–20Co–0.9Al–1.8Ti–2Nb–0.3Mn–0.7Fe–0.5Si and (balance) Ni. Ingots of the alloy were homogenized at 1204 °C for 16 h and hot worked at temperature above 1050 °C for 30 min. and then water-quenched. The standard precipitation treatment was made at 800 °C for 16 h and then air-cooled.[1] In the commercial-grade standard sample, the average size of grains and γ' precipitates are known to be about 50 μm and 40 nm, respectively.[1]

Thermo-mechanical treatment was carried out using a thermo-mechanical cycling equipment Gleeble 1500

[a)]Address all correspondence to this author.
e-mail: jijang@hanyang.ac.kr
DOI: 10.1557/jmr.2011.70

(Dynamic Systems Inc., Poestenkill, NY). The rectangular cuboid sample (5 mm × 6 mm × 12 mm) was heated up to 700 °C at a heating rate of 70 °C/s in an argon environment and then held at the peak temperature for 1 h under different levels of compressive stress: $\sigma = 0$, 300, and 800 MPa. Since the yield strength of the alloy is 648 MPa at 700 °C, 300 and 800 MPa are stresses in the "elastic" and "plastic" regime, respectively. After the thermo-mechanical treatment, the sample was quenched in air.

Microstructure was examined by using field emission scanning electron microscopy (JSM-6340F; JEOL Ltd., Tokyo, Japan). With the scanning electron microscopy (SEM) micrographs, the size and fraction of γ' were quantitatively measured using an image analyzer software (Image-pro; Media Cybernetics Inc., Bethesda, MD). An electrical etching (at 10 V for 90 s in a solution of 10 mL perchloric acid, 30 mL propionic acid, and 40 mL ethanol) and a chemical etching (for 10 s in a solution of 33 mL nitric acid and 66 mL hydrochloric acid) were adopted for measuring the size and fraction of γ', respectively. Adoption of different methods was because the electrical etching (that selectively etches out the γ matrix having a large fraction) could induce an overestimation of γ' fraction, whereas the chemical etching (that selectively etches out the γ matrix) could result in an overestimation of γ' size.

To investigate the mechanical properties, nanoindentation experiments were carried out using a Nanoindenter-XP (MTS System Corp., Oak Ridge, TN) with a common Berkovich indenter. During the test, the sample was loaded up to the peak load (P_{max}) of 10 mN under a constant strain rate of 0.05 s^{-1}. The tip calibration and the hardness calculation were conducted in accordance with the Oliver–Pharr method.[11] More than 10 indentation tests under each testing condition were made on electropolished samples instead of mechanically polished samples to avoid artifacts related to a hardened surface layer. The specimen surfaces were initially ground with fine SiC paper of no. 2000 and then electrically polished at 40 V for 20 s in a solution of 850 mL methanol and 150 mL hydrochloric acid at a room temperature.

III. RESULTS AND DISCUSSION

Representative SEM micrographs for the thermally treated only (i.e., $\sigma = 0$ MPa), the elastically stressed (300 MPa), and the plastically stressed (800 MPa) samples etched "electrically," and the measured size distribution of γ' precipitates are shown in Fig. 1. All samples exhibited very fine dispersion of spherical γ' precipitates in γ matrix. Using high resolution SEM images (×70,000), the size and fraction of γ' were investigated, with the results summarized in Fig. 2 (in which the SEM micrographs of the "chemically" etched samples are also provided). At least six high resolution micrographs were used for measuring the γ' fraction and more than 150 precipitates were examined for estimating the diameter of the spherical precipitates. In the figure, with increasing applied stress, the fraction of γ' continuously increased, whereas their diameter was not significantly changed and remained in the range of 20–60 nm (also see Fig. 1). As the γ' size is almost unchanged in the highly stressed sample, one might imagine that the increase in γ' fraction with the stress is mainly attributed to the enhanced nucleation of the γ' precipitates rather than their growth. Note that the time for the thermal–mechanical treatment (i.e., 1 h) is conceivably too short to induce proper precipitate coarsening.

The possible enhancement of γ' nucleation due to the external stress might be explained by taking into consideration the nucleation rate of a γ' precipitate and its Gibbs free energy barrier.[12] If the concentration of heterogeneous nucleation sites is C_1 per unit volume, the heterogeneous nucleation rate can be simply given as

$$J = fC_1 \exp\left(-\frac{\Delta G}{kT}\right) \quad , \tag{1}$$

where k and T are Boltzmann's constant and absolute temperature, respectively, f is a complex factor depending on how frequently a critical nucleus can receive an atom from the matrix, and ΔG is critical value of Gibbs free energy barrier for the nucleation that can be obtained from the classical theory of nucleation as

$$\Delta G = -V(\Delta G_V - \Delta G_S) + A\gamma - \Delta G_d \quad , \tag{2}$$

where V and A are the volume and surface area of precipitate, respectively, γ is the inter-phase interface energy, ΔG_v is the change in volume free energy, ΔG_s is the change in misfit strain energy, and ΔG_d is the amount of free energy that can be released by heterogeneous nucleation on crystalline defects (e.g., dislocations in the present work).

The external stress strains the material elastically or plastically, depending on the level of stress. In the case that the stresses do not surpass the yield stress, the resulting elastic strains may partially accommodate the misfit strain of (fully or partially) coherent precipitates, which results in the reduction of misfit strain energy term ΔG_s and thus the total free energy barrier (ΔG) in Eq. (2).[13] It is noteworthy that, although the portion of ΔG_s in ΔG can be small, the nucleation rate can be significantly enhanced by the change in ΔG_s because of the exponential dependence of the rate on the activation energy. Therefore, the elastic stress will certainly lead to the easier nucleation of γ' precipitates and thus increase in their fraction.

Much higher fraction of γ' precipitates in the plastically stressed sample might be associated with both increasing nucleation site and decreasing activation energy barrier; if the applied stresses are higher than the yield strength, the

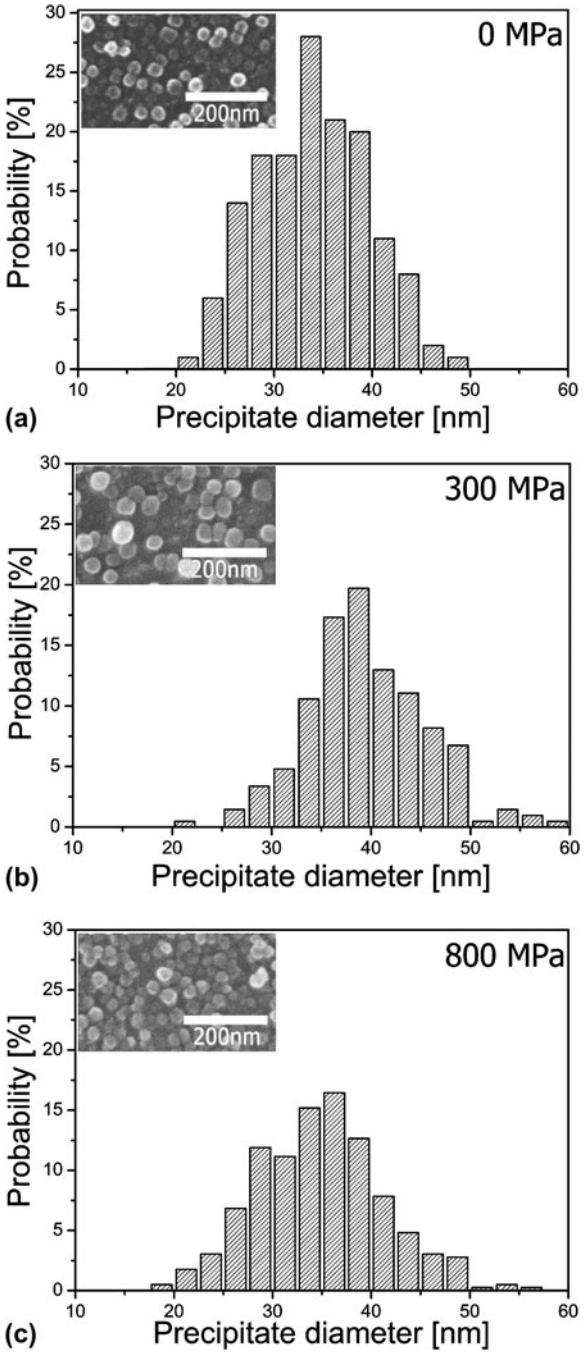

FIG. 1. Size distribution of γ' precipitates: (a) 0 MPa, (b) 300 MPa, and (c) 800 MPa. Inset images are examples of the SEM micrographs used for measuring the size of γ'.

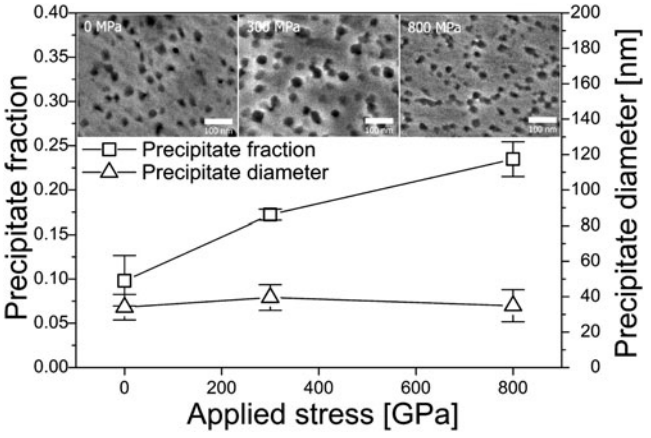

FIG. 2. Plot of γ' fraction and size with the stress applied at 700 °C. Inset images are examples of the SEM images used for measuring the fraction of γ'.

plastic deformation occurs and thus results in the multiplication of dislocation having excess line energies and an elastic stress field. The increased dislocation density can enhance the nucleation rate of the precipitates,[5,13–15] which may be explained by three mechanisms: first, the dislocation lines are interrupted by the nucleation of the precipitates, which shorten the dislocation and save dislocation line energies. Accordingly, this can induce the increase in the ΔG_d (which can be often considered as the dislocation core energy over the particle radius)[16] in Eq. (2) and hence the decrease in ΔG. This hypothesis is somewhat analogous to a mechanism suggested for hot-working-enhanced precipitation in a heat-resistant steel.[17] Second, if the particle misfit of coherent (or partially coherent) precipitates is accommodated by the elastic strain of the dislocation stress field (i.e., if there is an attractive interaction between the dislocation stress field and the particle stress field), ΔG_s and thus ΔG in Eq. (2) are reduced, which is similar to the effect of elastic stress. Third, for above reasons, dislocations are energetically preferential sites for heterogeneous nucleation of the precipitates. Thus, the dislocation density increase by plastic deformation can lead to the increase in the nucleation site concentration C_1 in Eq. (1) and the enhancement of the nucleation rate. Conclusively, the γ' fraction in the plastically stressed sample is much higher than that in the elastically stressed one.

Next, we turned our attention to the change in nanoindentation hardness by the thermo-mechanical treatment. For a given sample, all the indentations were made within a grain to exclude the influence of grain boundary strengthening, which also made it possible to avoid the grain orientation effect on the strength. Representative nanoindentation load–displacement (P–h) curves obtained at the peak load of 10 mN are shown in Fig. 3. It is evident that, as the applied stress increases, the maximum displacement at the peak load decreases, implying that hardness increases. The nanoindentation hardness measured from each sample was 7.36 ± 0.33 GPa for σ = 0 MPa, 7.74 ± 0.16 GPa for σ = 300 MPa, and 8.14 ± 0.17 GPa for σ = 800 MPa. From these results, it was convinced that the thermo-mechanical treatment did not induce any strength degradation and the strength is even enhanced by the treatment. Note that the obtained

nanoindentation hardness may be higher than conventional Vickers hardness (measured at much higher peak load) because of the well-known "indentation size effect," i.e., an increase in hardness with decreasing indentation load and depth.[18]

To analyze the way the precipitates might affect strengthening responsible for the hardness variation, the contribution of each strengthening mechanism was investigated in terms of the critical shear stress required for cutting or bowing. As mentioned earlier, precipitation strengthening in a superalloy is usually controlled by cutting mechanism that can be subdivided into two models, i.e., WCD model[9] for small particles and SCD model[10] for large particles. For both cases, it is possible to estimate the critical shear stress necessary for cutting the precipitates based on the assumptions that a pair of edge dislocations travels in the <110> direction on the {111} plane and cut through the ordered γ' precipitates in a disordered matrix.

In the case of WCD model appropriate for small particles, the critical shear stress for cutting can be given as[9]

$$\tau_{\mathrm{ppt,\,WCD}} = \frac{1}{2}\left(\frac{\gamma_{\mathrm{APB}}}{b}\right)^{\frac{3}{2}}\left(\frac{bdf}{T}\right)^{\frac{1}{2}}A - \frac{1}{2}\left(\frac{\gamma}{b}\right)f \quad , \qquad (3)$$

where γ_{APB} is the anti-phase boundary energy of the γ' in the {111} plane, b is the Burgers vector of edge dislocation in the matrix, d is the particle diameter, f is the volume fraction of the γ' particles, T is the line tension of the dislocation, and A is the numerical factor depending on the morphology of the particles (i.e., 0.72 for spherical particles).[6]

For SCD model applicable to larger particles, the critical shear stress can be obtained by[10]

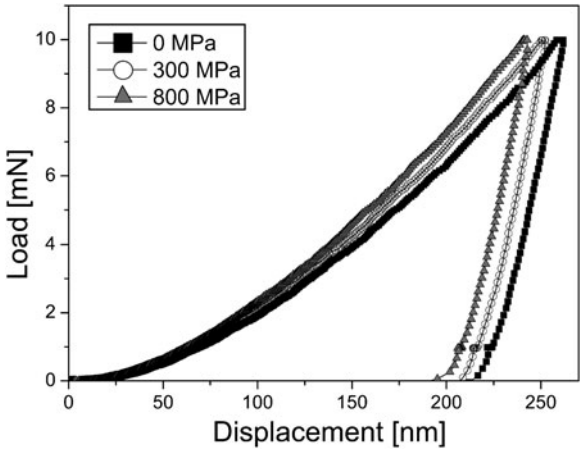

FIG. 3. Variations in nanoindentation load–displacement curve by the thermal–mechanical treatment.

$$\tau_{\mathrm{ppt,\,SCD}} = \left(\frac{\sqrt{3}}{2}\right)\frac{Tf^{\frac{1}{2}}w}{bd}\left(1.28\frac{d\gamma_{\mathrm{APB}}}{wT} - 1\right)^{\frac{1}{2}} \quad , \qquad (4)$$

where w is a constant (of the order of unity) that accounts for the elastic repulsion between the strongly paired dislocations[6] and is considered as unity in this work.

To calculate Eqs. (3) and (4), the value of b, γ_{APB}, G, and T should be known. In this study, b and γ_{APB} were taken as 0.254 nm and 0.28 J m^{-2}, respectively.[19] The shear modulus G [$= 0.5E/(1 + \nu)$] was calculated using elastic modulus E = 221 GPa (of Inconel 740) and Poisson's ratio ν = 0.35,[20] and T was estimated as $0.5Gb^2$.[9] It is noteworthy that recently many simulation works (e.g., see Ref. 21 and 22) have been made to provide the equations for more precisely calculating the critical shear stress for cutting in consideration of additional factors such as the long-range ordering and shapes of precipitates and the motion of the different-typed dislocations (i.e., screw and mixed dislocation). However, the effects of such factors have not been fully established yet and thus, in this work, we have taken the classical equations of (3) and (4) for simplifying calculations.

Although the cutting mechanism is known to be predominant mechanism for precipitation strengthening in a superalloy, previous works[23,24] reported that, in a limited condition (e.g., for large particles in an overaged condition), precipitation strengthening of superalloys can be also controlled by Orowan mechanism. It is well accepted that the critical stress necessary for Orowan (bowing) mechanism can be expressed as[25]

$$\tau_{\mathrm{ppt,\,Oro}} = \frac{Gb}{\lambda} \quad , \qquad (5)$$

where λ is interparticle spacing between precipitates and is often simplified as

$$\lambda = \frac{2(1-f)d}{3f} \quad , \qquad (6)$$

where f is the volume fraction of precipitates and d is the diameter of the spherical precipitate. As these f and d were already obtained experimentally (see Fig. 2), the critical shear stress required for Orowan mechanism can be easily evaluated according to Eqs. (5) and (6).

With the values of the critical shear stress calculated from Eqs. (3)–(5), one can estimate the contribution of each strengthening mechanism to the measured macroscopic hardness. By applying Tabor's relationship and von Mises flow rule, the critical stress values for each strengthening mechanism (τ_{ppt}) can be converted into the indentation hardness[26]:

$$H_{ppt} = 3\sigma_{ppt} = 3\sqrt{3}\tau_{ppt} \quad , \tag{7}$$

where H_{ppt} is the amount of hardness increase, thanks to the precipitation strengthening.

To find out the proper contributing mechanism, the τ_{ppt} for each mechanism was plotted with the particle diameter, which is given in Fig. 4. For this theoretical calculation, the fraction of precipitates was fixed as average values for each sample (see Fig. 2). In Fig. 4, for a given diameter, the mechanism showing the lowest τ_{ppt} value is supposed to mainly contribute to the strengthening. Note that the experimentally measured diameter was in the range of 20–60 nm. For all samples, with increasing particle size, there is a transition of the governing mechanism from WCD cutting to Orowan mechanism. The SCD cutting mechanism could be ruled out for entire range of particle diameter. In the figure, the maximum τ_{ppt} (at the transition point from the WCD cutting curve to Orowan curve) indicates the maximum possible amount of the particle strengthening. It is interesting to note that the maximum τ_{ppt} between WCD and Orowan curve increases more significantly with the applied stress vis-à-vis the value between WCD and SCD curve, i.e., the increase in the contribution of γ' to the strengthening with increase in the applied stress is more pronounced in WCD–Orowan case rather than in WCD–SCD case. This trend might arise from the fact that the τ_{ppt} for Orowan mechanism has higher sensitivity to volume fraction f than that for SCD cutting mechanism because the former and the latter are proportional to $f/(1-f)$ and $f^{0.5}$, respectively.

Finally, we have analyzed the contribution of H_{ppt} change to the overall hardness change. Total (overall) hardness H_{tot} can be described as

$$H_{tot} = H_{mat} + H_{ppt} \quad , \tag{8}$$

where H_{mat} is the matrix hardness, which is the strength term contributed by other sources rather than γ' precipitates (e.g., Peirls–Nabbaro stress, dislocation hardening, and solid solution strengthening by Co for this alloy). As mentioned earlier, grain boundary strengthening was excluded because all indentations were made at the interior of the grain. It is noteworthy that here we did not consider the role of carbides simply because their fraction is very low compared to γ' fraction (for all examined samples). Also, we could not find any other important feature of phase transformations such as η phase precipitation. Note that thermodynamically calculated equilibrium (not shown here) indicated that η phase is not stable at 700 °C. While H_{tot} was simply calculated from nano-indentation experiment according to Oliver–Pharr method,[11] H_{ppt} was determined in the following procedure: first, we directly compared the plot of size versus its fraction (Fig. 1) with the plot of size versus τ_{ppt} (Fig. 4) to determine which size corresponds to which mechanism (WCD or Orowan mechanism). Next, we calculated the τ_{ppt} for individual size in both the WCD regime and the Orowan regime according to Eqs. (3) and (5), respectively. Then, the overall τ_{ppt} was determined in consideration of τ_{ppt} of individual size and the fraction of each size. Finally, the obtained overall τ_{ppt} was converted to H_{ppt} by Eq. (7). Figure 5 exhibits the calculated H_{ppt} and H_{mat} together

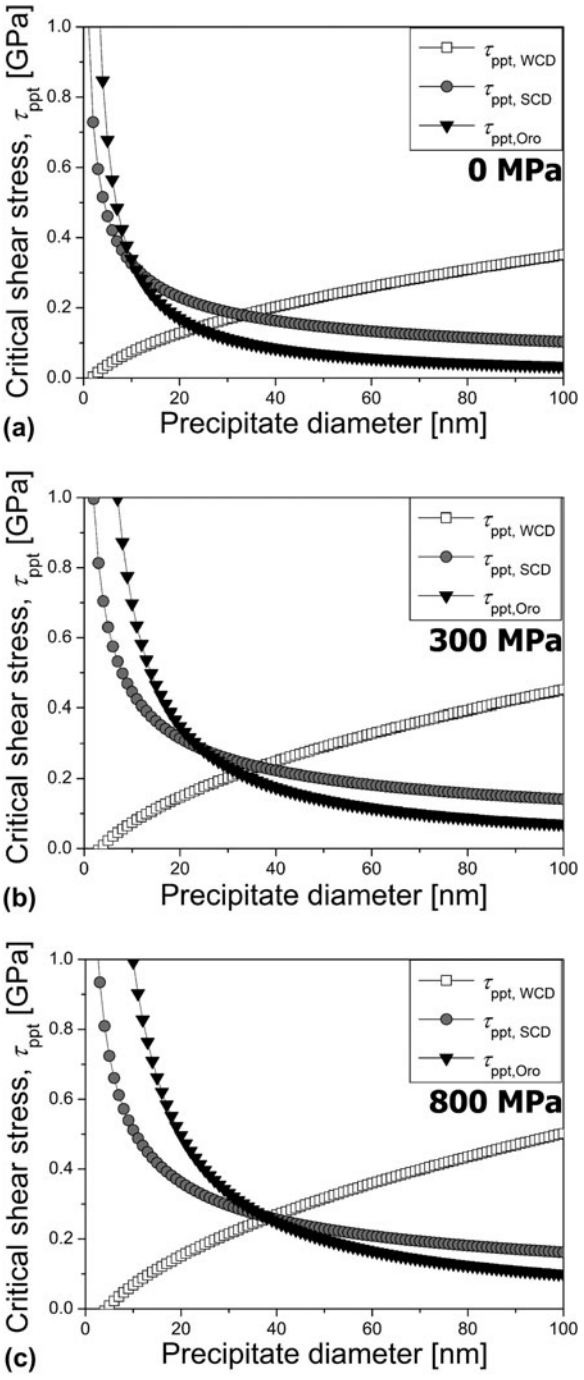

FIG. 4. Analytical calculations of the critical shear stress versus particle diameter: (a) 0 MPa, (b) 300 MPa, and (c) 800 MPa.

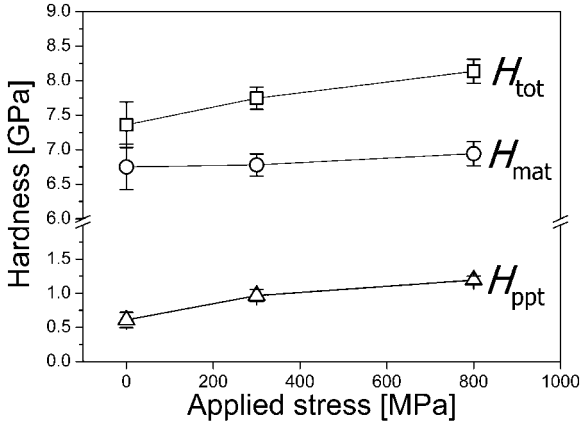

FIG. 5. Summary of the measured nanoindentation hardness (H_{tot}), the precipitation strengthening contribution to the hardening (H_{ppt}), and the calculated matrix hardness (H_{mat}).

with H_{tot}. It is obvious that the change in the H_{mat} with the stress is very small compared with that in the H_{ppt}. Especially, it is interesting to note that, although plastic deformation should increase the dislocation density and the strength (by strain hardening), the change in the average H_{mat} between 300 and 800 MPa sample (from ~6.78 to ~6.94 GPa) is smaller than that in the average H_{ppt} (from ~0.97 to ~1.19 GPa). From Fig. 5, it was believed that the overall strength enhancement by the thermo-mechanical treatment is seriously affected by the change in the amount of precipitation strengthening.

IV. CONCLUSION

The influence of the high stress at high temperature on the γ' precipitation behavior and its strengthening in Inconel 740 superalloy was investigated by using thermo-mechanically treated samples. Microstructural analysis revealed that, with increasing stress, the fraction of γ' precipitates increased but their size was not significantly changed and remained in the range of 20–60 nm, which might be understood by considering the effects of the external stresses and the resulting elastic/plastic strains on the free energy barrier and the concentration of the nucleation sites for heterogeneous nucleation. Measurement of nanoindentation hardness showed that the strength was enhanced by the thermo-mechanical treatment. The hardness variation could be explained by analyzing the critical stress values for the governing precipitation strengthening mechanisms (i.e., cutting versus bowing). By dividing the overall hardness H_{tot} into the matrix hardness H_{mat} and the contributing amount of precipitation strengthening H_{ppt}, it was proved that the change in the H_{ppt} was largely responsible for the overall strength enhancement by thermo-mechanical treatment.

ACKNOWLEDGMENT

This work was supported by the Human Resources Development of the Korea Institute of Energy Technology Evaluation and Planning (KETEP) grant funded by the Korea government Ministry of Knowledge Economy (No. 20101020300460).

REFERENCES

1. S. Zhao, X. Xie, G.D. Smith, and S.J. Patel: Microstructural stability and mechanical properties of a new nickel-based superalloy. *Mater. Sci. Eng. A* **355**, 96 (2003).
2. N.D. Evans, P.J. Maziasz, R.W. Swindeman, and G.D. Smith: Microstructure and phase stability in INCONEL alloy 740 during creep. *Scr. Mater.* **51**, 503 (2004).
3. J.E. King: Fatigue-crack propagation in nickel-base superalloys—effects of microstructure, load ratio, and temperature. *Mater. Sci. Technol.* **3**, 750 (1987).
4. B. Reppich, P. Schepp, and G. Wehner: Some new aspects concerning particle hardening mechanism in γ' precipitating Ni-Base alloys—II. Experiments. *Acta Metall.* **30**, 95 (1982).
5. P. Gopalan, R. Rajaaman, B. Viswanathan, K.P. Gopinathan, and S. Venkadesan: The kinetics of formation and growth of TIC precipitates in Ti-modified stainless steel studied by positron annihilation spectroscopy. *J. Nucl. Mater.* **256**, 229 (1998).
6. B. Reppich: Some new aspects concerning particle hardening mechanism in γ' precipitating Ni-Base alloys—I. Theoretical concept. *Acta Metall.* **30**, 87 (1982).
7. E. Nembach, K. Suzuki, M. Ichihara, and S. Takeuchi: In situ deformation of the γ' hardened superalloy Nimonic-PE16 in high-voltage electron-microscopes. *Philos. Mag.* **51A**, 607 (1985).
8. E. Nembach: *Particle Strengthening of Metals and Alloys* (John Willey and Sons, New York, 1996).
9. L.M. Brown and R.K. Ham: *Strengthening Methods in Crystals*, edited by K. Kelly and R.B. Nicholson (Applied Science, London, 1971), p. 12.
10. W. Huther and B. Reppich: Interaction of dislocations with coherent, stress-free, ordered precipitates. *Z. Metallk.* **69**, 628 (1978).
11. W.C. Oliver and G.M. Pharr: An improved technique for determining hardness and elastic-modulus using load and displacement sensing indentation experiments. *J. Mater. Res.* **7**, 1564 (1992).
12. D.A. Porter and K.E. Eastering: *Phase Transformations in Metals and Alloys* (Taylor & Francis Group, New York, 2004).
13. G. Sauthoff: Influence of stress on precipitation. *J. De Phy. IV* **6**, 87 (1997).
14. W. Kesternich: Microstructural evolution and mechanical-properties of advanced high-temperature steel. *J. Nucl. Mater.* **155**, 1025 (1988).
15. J.W. Cahn: Nucleation on dislocations. *Acta Metall.* **5**, 169 (1957).
16. B. Dutta, E.J. Palmiere, and C.M. Sellars: Modelling the kinetics of strain induced precipitation in Nb microalloyed steels. *Acta Mater.* **49**, 785 (2001).
17. J.-H. Kim, J.-H. Baek, C.-H. Han, S.-H. Kim, C.-B. Lee, K.-S. Na, and S.-J. Kim: Effect of thermomechanical process on mechanical property and microstructure of 9Cr-1Mo steel. *J. Korean. Inst. Met. Mater.* **47**, 621 (2009).
18. W.D. Nix and H. Gao: Indentation size effects in crystalline materials: A law for strain gradient plasticity. *J. Mech. Phys. Solids* **46**, 411 (1998).
19. M.P. Jackson and R.C. Reed: Heat treatment of UDIMET 720Li: The effect of microstructure on properties. *Mater. Sci. Eng. A* **259**, 85 (1999).
20. T. Pretorius and E. Nembach: Strengthening of an $L1_2$-ordered γ' intermetallic by disordered γ-particles. Part I: Computer simulations. *Acta Mater.* **49**, 1971 (2001).

21. V. Mohles: The critical resolved shear stress of single crystals with long-range ordered precipitates calculated by dislocation dynamic simulations. *Mater. Sci. Eng. A* **365**, 144 (2004).
22. S.I. Rao, T.A. Parthasarathy, D.M. Dimiduk, and P.M. Hazzledine: Discrete dislocation simulations of precipitation hardening in superalloys. *Philos. Mag.* **84**, 3195 (2004).
23. L. Brown: The self-stress of dislocations and the shape of extended nodes. *Philos. Mag.* **10**, 441 (1964).
24. U.F. Kocks: The theory of an obstacle-controlled yield strength. *Mater. Sci. Eng.* **27**, 291 (1977).
25. E. Orowan: Symposium on International Stresses (Inst. of Metal. London, 1947).
26. D. Tabor: *The Hardness of Metals* (Clarendon Press, Oxford, 1951).